Frequency Deadband Control of Grid-forming Energy Storage Inverter in Primary Frequency Regulation

Wei Zhang, Zhenxiong Wang, Yingjie Peng, Jingting Wu, Qiru Li, Hao Yi, Zebin Yang, Li Li, and Fang Zhuo

***Abstract*—With the increased penetration of renewable energy sources, the grid-forming (GFM) energy storage (ES) has been considered to engage in primary frequency regulation (PFR), often necessitating the use of a frequency deadband (FDB) to prevent excessive battery charging cycling and mitigate frequency oscillations. Implementing the FDB is relatively straightforward in grid-following (GFL) control. However, implementing the FDB in GFM control presents a significant challenge since the inverter must abstain from providing active power at any frequency within the FDB. Therefore, in this paper, the performance of PFR control in the GFM-ES inverter is analyzed in detail first. Then, the FDB is implemented for GFM inverters with various types of synchronization methods, and the need for inertia response is also considered. Moreover, given the risk of oscillations near the FDB boundary, different FDB setting methods are proposed and examined, where an improved triangular hysteresis method is proposed to realize the fast response and enhanced stability. Finally, the simulation and experiment results are provided to verify the effectiveness of the above methods.**

***Index Terms*—Primary frequency regulation (PFR), frequency deadband (FDB), grid-forming (GFM) control, energy storage (ES) inverter.**

I. Introduction

THE environment protection endeavor has been promoting the rapid expansion of sustainable and environment-friendly renewable energy sources (RESs) [1], [2]. The RES typically works in the maximum power point tracking mode, resulting in the power fluctuation problem [3]. Energy storage (ES) inverters, with bi-directional power transmission and fast response capability, can suppress random and frequent power fluctuations, which are gradually used in auxiliary service [4].

Currently, most ES inverters are integrated into the power grid in the grid-following (GFL) mode. However, in some regions with very high penetration of RESs, severe stability issues may arise in weak grids [5]. This GFL control utilizes the voltage phase derived from the phase-locked loop (PLL) to facilitate effective power tracking. The power reference for primary frequency regulation (PFR) is conventionally disseminated by a central controller through dedicated communication lines. The central controller serves as an integrative mechanism that facilitates real-time communication among multiple inverters, ensuring a coordinated response to frequency deviations [6]. Nonetheless, the GFL control method necessitates a central controller with high computational and communication speeds. When faced with deteriorating frequency quality and grid voltage fluctuations, this method encounters substantial challenges in terms of response time and the ability to support grid voltage [7].

Therefore, the grid-forming (GFM) control is considered in the recent deployment of ES to deeply participate in the voltage/frequency support. The droop control is a well-known method that realizes voltage/frequency support and reasonable power allocation among different inverters [8]. Moreover, the virtual synchronous generator (VSG) is also a well-known method that can lower the rate of change of frequency (RoCoF) in the transient state by adding virtual inertia to the *P-f* droop control loop [9]. According to recent findings, the GFM inverter performs better in weak grids regarding stability enhancement, transmission of renewable energy over long distances, and voltage/frequency support. Regarding different synchronization methods to realize the PFR and inertia control, the power synchronization control (PSC) and DC voltage synchronization control (DVSC) can be used in the ES inverter [10], [11]. The GFM converter with the DVSC method has a better physical equivalence with the synchronous generator (SG). The size of the DC-side capacitance is equivalent to the inertia constant of the synchronous generator (SG), while the DC voltage is equivalent to the rotational speed of the SG rotor [12].

PFR is one of the auxiliary services to realize fast power balance and frequency maintenance. In the PFR, the output

Manuscript received: July 17, 2024; revised: October 26, 2024; accepted: December 17, 2024. Date of CrossCheck: December 17, 2024. Date of online publication: January 30, 2025.

This work was supported by the Science and Technology of State Grid (No. 4000-202432066A-1-1-Z).

W. Zhang, Z. Wang (corresponding author), Y. Peng, J. Wu, Q. Li, H. Yi, Z. Yang, and F. Zhuo are with the School of Electrical Engineering, Xi'an Jiaotong University, Xi'an 710049, China (e-mail: zhang-wei@stu. xjtu. edu. cn; wzhenxiong@xjtu.edu.cn; engyingjie@stu.xjtu.edu.cn; jtkathy958@stu.xjtu. edu. cn; liqr0912@stu. xjtu. edu. cn; yi_hao@xjtu. edu. cn; yangzebin@xjtu. edu. cn; zffz@mail.xjtu.edu.cn).

L. Li is with the State Grid Shaanxi Electric Power Company, Xi'an 710049, China (e-mail: 33066410@qq.com).

DOI: 10.35833/MPCE.2024.000757

power and frequency must adhere to a predefined curve, typically comprising a droop area, frequency deadband (FDB), and saturation area [13]. Due to fluctuations in short-term load demands and the inherent variability of RESs, minor perturbations frequently occur in the power grid, leading to frequency oscillations near the nominal range. Therefore, the governors of SGs need an FDB to mitigate unnecessary operations and reduce wear and tear [14]. In China, the typical FDBs of hydropower units and thermal power units are ±0.05 Hz and ±0.033 Hz, respectively. Similarly, the ES inverters also need an FDB to avoid the frequent charging and discharging, thereby extending their lifespans and minimizing unnecessary frequency adjustments. Hence, it is crucial to properly set the FDB size and select the FDB types for ES inverters.

Conventionally, SGs participate in PFR with the frequency governor of the prime mover after the release of rotor kinetic energy [15]. However, the response speed of SG is relatively slow due to the mechanical delay of the prime mover [16]. Currently, the ES inverter usually operates in the GFL mode, wherein implementing PFR is straightforward as the inverter merely needs to track the setpoint defined by the *P-f* curve [17]. For example, the GFL inverter can easily achieve zero power response within the FDB by simply setting the current reference to zero. In [18], considering the limitations of the state of charge (SOC) of ES, the droop coefficient and FDB size setting are discussed. Reference [19] proposes a step FDB to enhance the fast and accurate response capabilities of the ES inverter. However, in the above-mentioned methods, the algorithm is executed on a central controller, which then issues a power command to the GFL-ES inverters for power tracking. The adaptation of FDB methods specifically for GFM-ES inverters has not been addressed.

When the GFM-ES inverter engages in the PFR, its output power is adjusted indirectly through the manipulation of the terminal voltage. Consequently, the current is not directly controlled, posing challenges to precise power control [20]. The implementation of a droop control is relatively straightforward within this control framework; however, achieving a precise FDB and saturation control proves to be a more formidable task. As shown in Fig. 1, within the FDB, zero power output corresponds to a frequency range. Nevertheless, in a GFM inverter, frequency serves as a setpoint for an internal control loop. Herein lies the issue: a range cannot serve as a definitive control command; otherwise, it would introduce substantial control complexities.

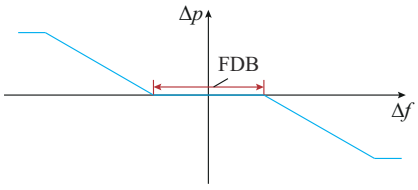

Fig. 1. Diagram of PFR with FDB.

Regarding the FDB control in GFM-ES inverters, the pivotal challenge lies in maintaining zero active power output within the specified FDB. This aspect has received limited attention in prior studies. The issue can be recast as the quest for precise and rapid control of the output current of GFM inverter, a topic that has garnered more research efforts. For example, after an overload or a grid fault, the GFM-ES inverters need current limiting control in the transient state [21]. In [22] and [23], the current is directly limited with a saturation module after the voltage loop to revise the current reference in the *dq* frame. In [24], an indirect current limiting method is proposed, where the virtual impedance increases in the transient state in the voltage loop. However, these approaches are not well-suited for power regulation within the FDB. This is because the current limiting control is primarily designed for abnormal transient conditions, where the voltage synchronization is significantly compromised due to the temporary suspension of the power control loop. Conversely, functioning within the FDB is a sustained normal operational mode that necessitates stringent voltage synchronization. Furthermore, devising a control strategy for zero power response within the FDB needs to consider variations in system configurations and different GFM topologies.

In this paper, the improved FDB control of the GFM-ES inverter is proposed. Firstly, the PFR performance of the GFM-ES inverter is investigated in detail. Then, the zero power response strategies suitable for GFM-ES inverters with different synchronization methods (i. e., DVSC and PSC methods) within the FDB are proposed. Furthermore, different FDB setting methods are proposed to enhance the PFR capability of the GFM-ES inverter and reduce oscillations near the FDB boundary. Finally, the simulation and experiment results are given for verification. These methods address the critical barriers in the FDB control of the GFM-ES inverter, and the main work and contributions are summarized as follows.

1) The PFR performance of GFL-ES and GFM-ES inverters are investigated and compared to quantify the merits of GFM-ES in PFR, especially under different grid strengths.

2) Two distinct methods for implementing FDB with different inertia responses (IRs) have been proposed to cater to different application scenarios: ① the power-reference-based (PRB) method, which is further categorized into AC- and DC-side strategies, and ② the ES output point (EOP) voltage-frequency-based (EVFB) method. The two methods can be applied to GFM-ES inverters with different topologies, synchronization methods, and IR demands, where all of them can realize almost zero power response in the steady state within the FDB.

3) To enhance the PFR performance of the GFM-ES inverter, a step FDB with triangular hysteresis method is presented, which can accelerate the response speed in PFR and suppress the oscillation near the FDB boundary.

II. Difference of GFL-ES and GFM-ES Inverters when Participating in PFR

A. Control Scheme for ES Inverter when Participating in PFR

The control structure of a three-phase grid-connected ES inverter is illustrated in Fig. 2, where PI is short for propor-

tional and integral; PWM is short for pulse width modulation; and RPC is short for reactive power controller. Notably, the DC voltage is set to be constant as the inverter control in PFR is mainly studied. The variables related to the non-control part of the grid-connected ES inverter are described in Supplementary Material A.

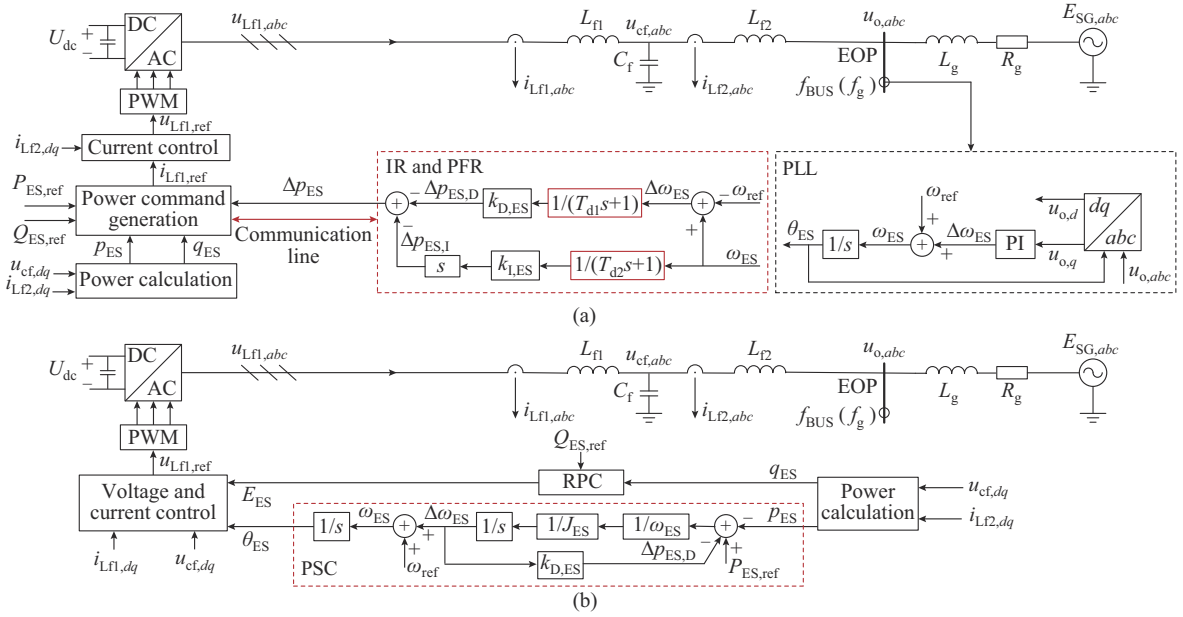

Fig. 2. Control structure of a three-phase grid-connected ES inverter. (a) GFL-ES inverter. (b) GFM-ES inverter.

The control structure of the GFL-ES inverter is shown in Fig. 2(a), which includes the PLL, IR, and PFR controllers, power calculation and power command generation modules, and inner current control loop. In contrast, the GFM-ES inverter shown in Fig. 2(b) uses the PSC loop for synchronization. Notably, the GFM-ES inverter omits the need for an explicit power command, as the power response is inherently adaptive to the changes of the grid voltage. Furthermore, the participation of GFL inverters in PFR is generally achieved by using a central controller to facilitate power allocation between the plant and individual inverters via communication during a disturbance. Therefore, in GFL inverters, the IR and PFR are typically realized within a centralized control architecture. Conversely, in GFM inverters, the implementation of IR and PFR is integrated directly into the local control loop, thereby eliminating the need for a separate central controller.

B. Active Power Response Analysis for ES Inverter

Currently, PFR primarily relies on the central controller applied as a fast frequency control manager, which involves command transmission from the station to the individual inverter, and this command transmission introduces the time delay e^{-ts}. Neglecting the higher-order terms of the time delay, it can be approximated as a first-order inertial element $1/(T_{d1}s+1)$, as shown in Fig. 2(a). During sudden power disturbances, both the frequency and RoCoF from PLL measurements experience abrupt changes, leading to suboptimal dynamic performance. The PLL struggles to accurately measure the actual frequency and RoCoF, which reduces the inertia support power supplied by the ES, diminishing the effectiveness of inertia control in the GFL method. To address this challenge, this paper was inspired by using the first-order high-pass filter, denoted as $s/(T_{d2}s+1)$, as shown in IR and PFR module in Fig. 2(a). This approach helps mitigate oscillations and fluctuations, thereby improving the IR ability.

The power response of GFL-ES inverter to frequency changes is given by:

$$\hat{p}_{ES}=-\frac{1}{T_{d1}s+1}k_{D,ES}\hat{\omega}_{ES}-\frac{1}{T_{d2}s+1}k_{I,ES}\frac{d\hat{\omega}_{ES}}{dt} \tag{1}$$

where $k_{D,ES}$ and $k_{I,ES}$ are the droop coefficient and virtual inertia, respectively; ω_{ES} is the angular frequency of ES inverter; p_{ES} is the output power of ES inverter; and the symbol $\hat{}$ represents the increment of the corresponding variable.

For the GFM-ES inverter, the frequency control is fundamentally governed by the PSC loop, as illustrated in Fig. 2(b). The control structure here embodies the principle of a VSG, wherein IR is inherently considered. When the frequency differential is excluded from the control algorithm, the system reverts to a conventional droop control. The PSC loop can be depicted as:

$$\hat{p}_{ES}=-k_{D,ES}\hat{\omega}_{ES}-J_{ES}\omega_{ref}\frac{d\hat{\omega}_{ES}}{dt} \tag{2}$$

where J_{ES} is the virtual inertia; and ω_{ref} is the reference angular frequency.

The difference between (1) and (2) is that the GFL-ES inverter has an uncertain delay, and the relationship of J_{ES} and $k_{I,ES}$ can be written as (3) if ignoring the delay of low-pass filter.

$$k_{I,ES}=J_{ES}\omega_{ref} \tag{3}$$

The time delay impacts on the GFL-ES inverter connected to an SG with limited capacity are analyzed, which means the SG itself has PFR capability. Figure 3 shows the dynamic PFR of the GFL-ES inverter with different delay time T_{d1}

and GFM-ES inverter considering a load step increase of 0.01 p.u., where f_{BUS} is the frequency of the AC bus, which is also called grid frequency f_g. Though the PLL is not used for PFR control in the GFM-ES inverter, as shown in Fig. 2(b), it is still employed for observation to ensure the fairness of comparison between the GFL-ES inverter and GFM-ES inverter. It is evident that as T_{d1} increases, the GFL inverter experiences a notable increase in both RoCoF and frequency deviations, which means a smaller T_{d1} can support the frequency more quickly and decrease the frequency nadir. Furthermore, Fig. 3 reveals that the performance of the GFM-ES inverter remains superior, even when T_{d1} in the GFL-ES inverter is reduced to an anomalous value of 0.005 s, i.e., a duration much shorter them typical PFR communication delays within RES stations.

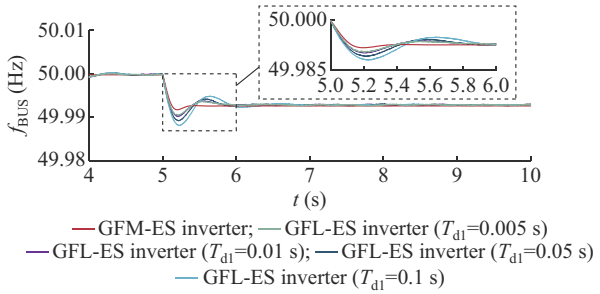

Fig. 3. Dynamic PFR of GFL-ES inverter with different T_{d1} and GFM-ES inverter.

The impact of the time constant T_{d2} is also investigated, as shown in Fig. 4. The simulation outcomes of f_{BUS} with GFL-ES inverter show that smaller T_{d2} will lead to increased frequency oscillations, but even if T_{d2} is large enough, the PFR performance of GFL-ES inverter is also worse than that of the GFM-ES inverter.

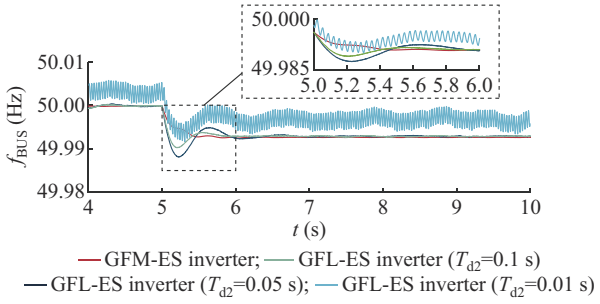

Fig. 4. Dynamic PFR of GFL-ES inverter with different T_{d2} and GFM-ES inverter.

After choosing suitable T_{d1} and T_{d2}, the dynamic PFR in weak grids is examined, where the SCR serves as an indicator of grid strength, and a decreasing SCR means a weakening grid. As depicted in Fig. 5, we compare the dynamic PFR of GFM-ES and GFL-ES inverters with different SCRs. As shown in Fig. 5(a), for the GFM-ES inverter, the grid frequency exhibits a relatively low sensitivity to variations in the SCR. However, as illustrated in Fig. 5(b), the GFL-ES inverter exhibits pronounced RoCoF and increased frequency deviation when the SCR decreases, despite the utilization of optimized T_{d1} and T_{d2} settings. This highlights the vulnerability of GFL-ES inverter to grid weakness. Therefore, the PFR of GFM-ES inverter is important, which is introduced in the following sections.

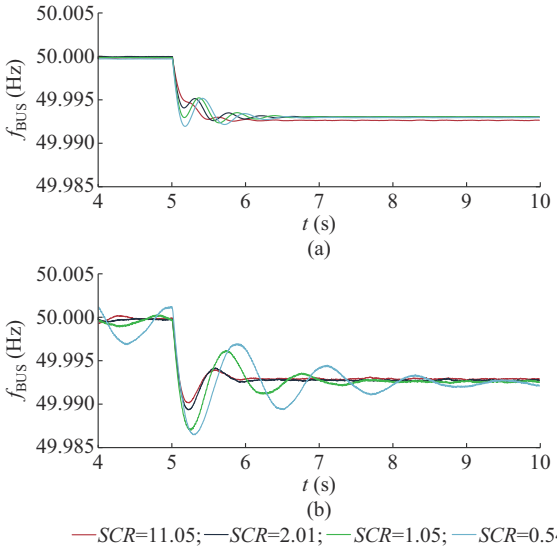

Fig. 5. Dynamic PFR of GFM-ES and GFL-ES inverters with different SCRs. (a) GFM-ES inverter. (b) GFL-ES inverter.

III. Implementation of FDB for Different Types of GFM-ES Inverters

In the GFM-ES inverter, the active power is determined by the voltage phase difference between the inverter terminal and EOP. This feature will cause continuously active power change within the FDB, potentially leading to a diminished ES service life and exacerbating frequency oscillations. Therefore, this section discusses how to implement FDB for different types of GFM-ES inverters.

As shown in Fig. 6, the ES inverters are typically categorized into two primary architectures: ① single-stage and ② two-stage configurations, which are with and without DC/DC pre-stages, respectively. Notably, the PSC method can be used in both types of ES inverters, while the DVSC method is exclusively applicable to the two-stage configuration. The implementation of FDB is studied for GFM-ES inverters with both methods.

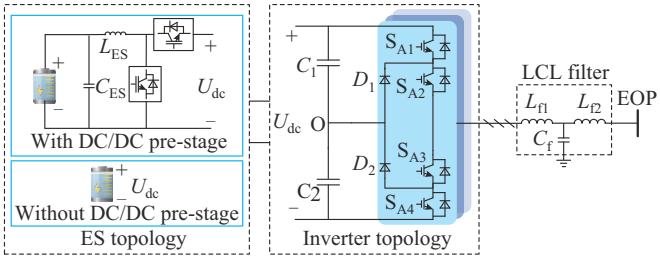

Fig. 6. Typical topology of grid-connected ES inverter.

A. Implementation of FDB for GFM-ES Inverter with DVSC Method

1) DVSC Method

The active power response of SG can be derived with the model shown in Fig. 7.

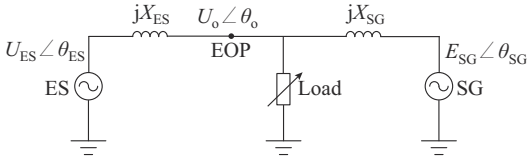

Fig. 7. Typical model of grid-connected ES inverter.

The relationship between the angular frequencies of EOP ω_o and SG ω_{SG} is written as [25]:

$$\begin{cases} \dfrac{\hat{\omega}_{SG}}{\hat{\omega}_o} = \dfrac{1}{1+\dfrac{k_{D,SG}}{k_{p,SG}}s+\dfrac{J_{SG}\omega_{ref}}{k_{p,SG}}s^2} \\ k_{p,SG} = \dfrac{3E_{SG}U_o}{2X_{SG}} \end{cases} \tag{4}$$

where $k_{D,SG}$, $k_{p,SG}$, J_{SG}, E_{SG}, U_o, and X_{SG} are the droop coefficient, power coefficient, rotor inertia of SG, voltage of SG, voltage of EOP, and line impedance on SG side, respectively.

The control structure of DVSC method is shown in Fig. 8,

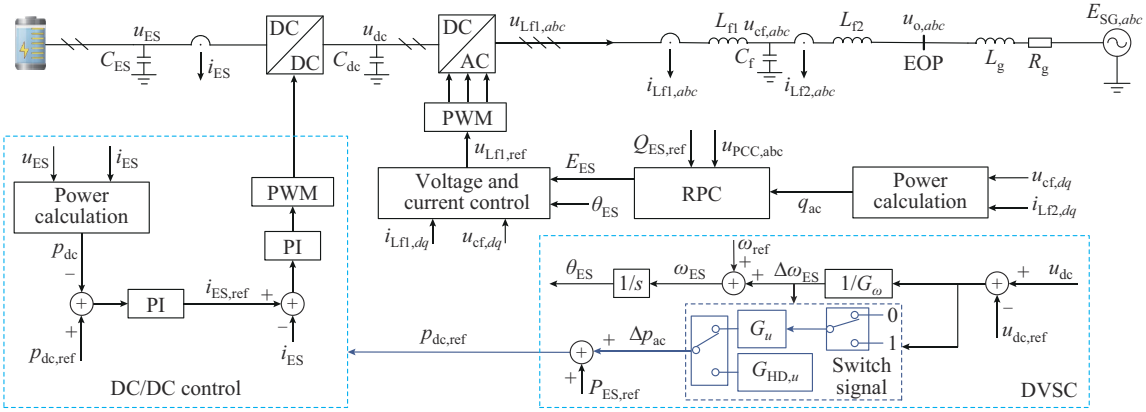

Fig. 8. Control structure of DVSC method.

According to (6), the physical meaning of the DVSC method is clear, and it can be used for guiding the design of virtual inertia J_{ES} and droop coefficient of ES $k_{D,ES}$.

2) DC-side PRB Method

For the GFM-ES inverter with DVSC method, the FDB is implemented by modifying the DC-side power reference $p_{dc,ref}$, and then the DC/DC control loop is used to track $p_{dc,ref}$ with a inner current loop. As shown in Fig. 8, a switch signal is added to realize zero power response. The switch signal is determined by whether the magnitude of the frequency deviation is within the FDB. As shown in Fig. 9, taking the triangular hysteresis as an example, when the frequency variation falls within the FDB, the switch signal is set to be 0; otherwise, it is set to be 1. Furthermore, if the frequency deviation transitions from being outside the FDB to within it, yet remains within the triangular hysteresis area, the calculated droop coefficient $G_{HD,u}$ is renewed and utilized.

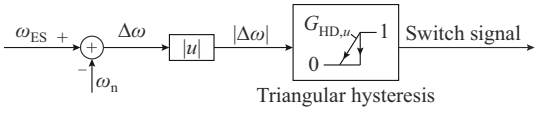

Fig. 9. Switch signal module of triangular hysteresis.

where the relationship between ω_o and angular frequency of ES ω_{ES} can be written as (5), which has been introduced in [26].

$$\begin{cases} \dfrac{\hat{\omega}_{ES}}{\hat{\omega}_o} = \dfrac{1}{1-\dfrac{G_u G_\omega}{k_{p,ES}}s-\dfrac{C_{dc}U_{dc}G_\omega}{k_{p,ES}}s^2} \\ k_{p,ES} = \dfrac{3U_{ES}U_o}{2X_{ES}} \end{cases} \tag{5}$$

where $k_{p,ES}$, U_{ES}, X_{ES}, C_{dc}, and U_{dc} are the power coefficient of ES, voltage of ES inverter terminal, line impedance on the ES side, capacitance of DC capacitor, and DC rated voltage, respectively; and the temporary variables G_ω and G_u can be obtained as (6) by comparing (4) and (5) to imitate the characteristic of SG.

$$\begin{cases} G_\omega = \dfrac{J_{ES}\omega_{ref}}{C_{dc}U_{dc}} \\ G_u = -\dfrac{C_{dc}U_{dc}k_{D,ES}}{J_{ES}\omega_{ref}} \end{cases} \tag{6}$$

The FDB size is determined based on the current field application status of PFR and the requirements for the participation of RES in PFR. The triangular hysteresis size is determined by considering the need to suppress frequency oscillations and reduce the number of ES charging and discharging cycles.

Within the FDB, the post-stage power increment Δp_{ac} is equal to zero as the switch signal is 0. Therefore, setting the post-stage power reference $P_{ES,ref}=0$, the DC-side power reference $p_{dc,ref}$ will equal zero, and the zero power response for PFR will be realized within the FDB. It should be noted that with the DC-side PRB method, the ES inverter can also provide IR through the DC capacitor instead of the ES within the FDB as the $1/G_\omega$ is related to the inertia J_{ES}, which also helps reduce unnecessary cycling of ES.

B. Implementation of FDB for GFM-ES Inverter with PSC Method

1) PSC Method

The control structure of the PSC method is illustrated in Fig. 10.

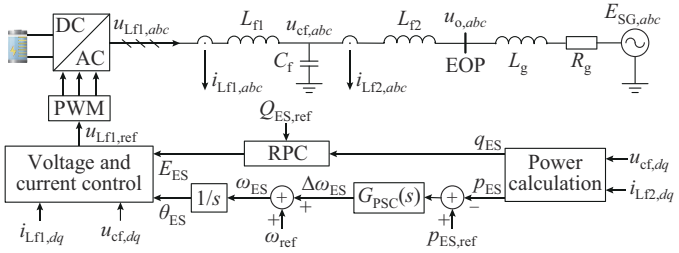

Fig. 10. Control structure of PSC method.

Based on the quasi-static model, the dynamic relationship between the active power response and grid frequency disturbance can be expressed as:

$$\begin{cases} p_{\mathrm{ES}} = k_{\mathrm{p,ES}}\delta \\ \delta = \theta_{\mathrm{ES}} - \theta_{\mathrm{o}} \end{cases} \tag{7}$$

where δ is the difference between the voltage phases of ES inverter terminal θ_{ES} and EOP θ_{o}.

In the time domain, the voltage phases of the ES inverter terminal and EOP can be expressed as (8). By combining (7) and (8), the relationship between δ and reference angle for active power control δ_{ref} in the time domain can be formulated as (9).

$$\begin{cases} \theta_{\mathrm{o}}(t) = \omega_{\mathrm{o}} t \\ \theta_{\mathrm{ES}}(t) = \omega_{\mathrm{ref}} t + \delta_{\mathrm{ref}}(t) \end{cases} \tag{8}$$

$$\delta_{\mathrm{ref}}(t) = (\omega_{\mathrm{o}} - \omega_{\mathrm{ref}})t + \delta(t) \tag{9}$$

From (9), different ω_{ref} will influence the output active power in steady states, which can be illustrated by (10). Therefore, setting the droop coefficient of ES $k_{\mathrm{D,ES}}$ to zero or ω_{ref} to ω_{o} will enable the implementation of FDB.

$$p_{\mathrm{ES}} = P_{\mathrm{ES,ref}} - k_{\mathrm{D,ES}}(\omega_{\mathrm{o}} - \omega_{\mathrm{ref}}) \tag{10}$$

2) AC-side PRB Method

As shown in Fig. 11, the AC-side power reference can be modified to mimic the DC-side PRB method. This method sets the droop coefficient $k_{\mathrm{D,ES}}$ to zero. Typically, there are two types of control methods for the PSC method: VSG and droop control. Both utilize the same switch signal module of the triangular hysteresis, as illustrated in Fig. 9, to implemente the FDB.

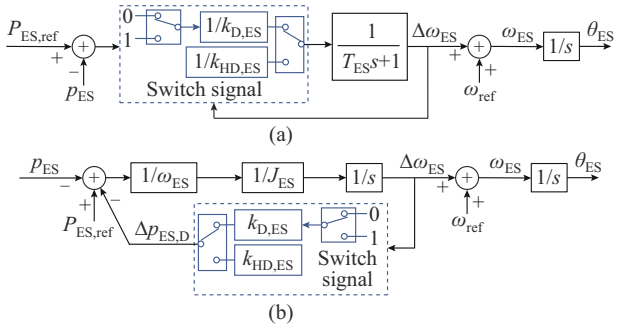

Fig. 11. AC-side power reference modifications. (a) Droop control. (b) VSG control.

In the VSG control, the switch signal module is incorporated into the feedback loop of the *P-f* droop control, while the IR remains active. Then, the power increment $\Delta p_{\mathrm{ES,D}}$ changes to zero when the frequency deviation is within the FDB. Herein, the IR unit inherently functions as an integral control loop to track the power reference of ES $P_{\mathrm{ES,ref}}$ that is set to be zero in this state. This implies that the VSG control realizes zero power output within the FDB in steady state while IR is still active. It should be noted that AC-side PRB method cannot be applied to the droop control shown in Fig. 11(a). This is because the control loop will break if $\Delta\omega_{\mathrm{ES}}$ equals zero within the FDB, especially with the absence of an inertia-based integral unit.

C. Implementation of FDB for GFM-ES Inverter with EVFB Method

In the EVFB method, the frequency reference ω_{ref} changes to ω_{ME} within the FDB, using a PLL for frequency measurement. Figure 12(a) illustrates the switch signal selection module, which comprises a PLL and a triangular hysteresis. The Quasi-static model for active power response is shown in Fig. 12(b). Equation (10) is modified to (11) with frequency reference ω_{n}, showing that the output active power is proportional to the deviation $\omega_{\mathrm{o}} - \omega_{\mathrm{n}}$.

$$p_{\mathrm{ES}} = P_{\mathrm{ES,ref}} - k_{\mathrm{D,ES}}(\omega_{\mathrm{o}} - \omega_{\mathrm{n}}) \tag{11}$$

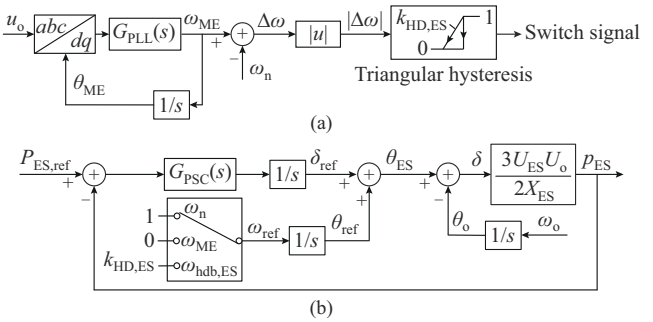

Fig. 12. EVFB method for FDB. (a) Switch signal selection module. (b) Quasi-static model for active power response.

The measured frequency ω_{ME} is captured from ω_{o}, and then (10) is modified as:

$$p_{\mathrm{ES}} = P_{\mathrm{ES,ref}} - k_{\mathrm{D,ES}}(\omega_{\mathrm{o}} - \omega_{\mathrm{ME}}) \tag{12}$$

In the steady state, the measured frequency ω_{ME} equals ω_{o}. Consequently, the actual output power is equal to the power reference $P_{\mathrm{ES,ref}}$. Therefore, the GFM-ES inverter with the EVFB method does not participate in the PFR within the FDB after setting $P_{\mathrm{ES,ref}} = 0$.

Notably, the EVFB method can be applied to both VSG and droop control, and it also can be utilized in the DVSC method as all the GFM control methods have a similar relationship shown in (10). Compared with the PRB method, the key difference is that the EVFB method can reduce the IR within the FDB, as the terminal frequency is directly fed back into the control loop, and the IR is only provided in the transient state for the control delay.

In summary, two types of methods for the implementation of FDB have been proposed to cater to different application scenarios: ① the PRB method, which is further categorized into AC- and DC-side PRB methods, and ② the EVFB method. The PRB method activates the IR while the EVFB method does not activate IR within the FDB to satisfy different IR requirements. The following conclusions can be drawn.

1) The DC-side PRB method is applicable in two-stage topologies utilizing the DVSC method, whereas the AC-side PRB method is utilized for VSG control.

2) The EVFB method for FDB is universally applicable to GFM-ES inverters.

IV. Configuration of FDB

This section discusses the configuration of various types of FDB mechanisms and proposes an improved triangular hysteresis based FDB setting method, particularly aiming at enhancing the system dynamic response and eliminating oscillations near the FDB boundary.

A. FDB Setting Method

Figure 13 shows four different FDB setting methods. Figure 13(a) shows a normal deadband (NBD) in which the output power begins to increase from zero when the frequency deviation exceeds the FDB. This FDB setting method is generally used for the conventional SG because the response speed is slow. To enhance the PFR capability of the ES inverter, the step deadband (SDB) shown in Fig. 13(b) is adapted. When the frequency deviation is outside the FDB, a fast step response can accelerate the desired frequency response and also reduce frequency deviation in the steady state. However, this control method may lead to oscillations near the FDB boundary, especially when the ES inverter operates in the GFM mode. To deal with the oscillation problem, a rectangular hysteresis is usually added to the step deadband, termed RHSDB, as shown in Fig. 13(c), which can reduce the oscillation near the FDB boundary.

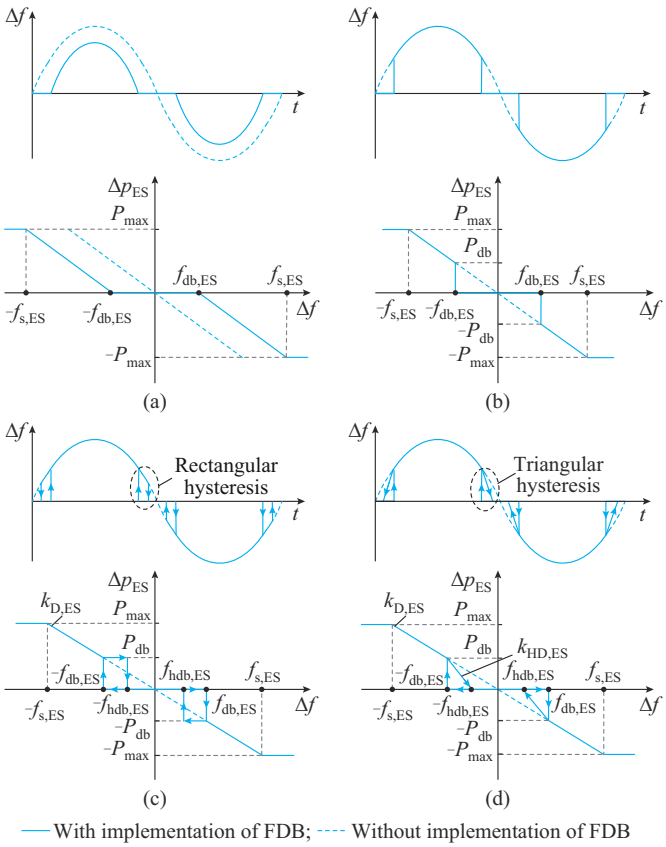

Fig. 13. FDB setting methods. (a) NBD. (b) SDB. (c) RHSDB. (d) THSDB.

The RHSDB method is expressed as:

$$\Delta p_{ES}=\begin{cases}0 & |\Delta f|<f_{hdb,ES}\\ 0 & f_{hdb,ES}<|\Delta f|<f_{db,ES},\Delta f\dot{\Delta f}>0\\ P_{db}\,\mathrm{sgn}(\Delta f) & f_{hdb,ES}<|\Delta f|<f_{db,ES},\Delta f\dot{\Delta f}<0\\ k_{D,ES}\Delta f & f_{db,ES}<|\Delta f|<f_{s,ES}\\ P_{max}\,\mathrm{sgn}(\Delta f) & |\Delta f|>f_{s,ES}\end{cases}\tag{13}$$

where $f_{hdb,ES}$, $f_{db,ES}$, and $f_{s,ES}$ are the boundaries of the hysteresis, FDB, and saturation areas, respectively; P_{db} and P_{max} are the output power values in the hysteresis and saturation areas, respectively; Δf and Δp_{ES} are the frequency deviation and related power increment, respectively; and sgn(·) is the signum function.

The rectangular hysteresis method needs a larger hysteresis band to prevent oscillation more effectively. However, this will deteriorate the performance both in droop and deadband states. To address the aforementioned issues, an enhanced triangular hysteresis method in step deadband, which is termed THSDB, is proposed, as shown in Fig. 13(d), which can be mathematically represented by (14). This control method employs a vertical transition when frequency moves from the FDB to the droop area, thereby expediting the system response time. Conversely, a diagonal line is utilized when returning from the droop area to the FDB, which moderates the RoCoF near the FDB boundaries, thus dampening oscillations. This allows active power adjustments through an additional droop curve in this area and the frequency reference equals $f_n \pm f_{hdb,ES}$. The THSDB method effectively mitigates oscillation that occurs near the FDB boundary and reduces the need for larger hysteresis margins.

$$\Delta p_{ES}=\begin{cases}0 & |\Delta f|<f_{hdb,ES}\\ 0 & f_{hdb,ES}<|\Delta f|<f_{db,ES},\ \Delta f\dot{\Delta f}>0\\ k_{HD,ES}\left|\Delta f-f_{hdb,ES}\right|\mathrm{sgn}(\Delta f) & f_{hdb,ES}<|\Delta f|<f_{db,ES},\ \Delta f\dot{\Delta f}<0\\ k_{D,ES}\Delta f & f_{db,ES}<|\Delta f|<f_{s,ES}\\ P_{max}\,\mathrm{sgn}(\Delta f) & |\Delta f|>f_{s,ES}\end{cases}\tag{14}$$

In summary, the EVFB method with triangular hysteresis is suitable for both DVSC and PSC methods. The PRB method with triangular hysteresis can be applied in the DVSC and VSG methods.

B. Triangular Hysteresis Size

The triangular hysteresis size should not be excessively large. Currently, the mechanical FDB, the minimum FDB of RESs, and the frequency deviation experienced under disturbances are approximately 0.02 Hz [18]. Therefore, the boundary for the THSDB can be set as 0.02 Hz, which means $|f_{hdb,ES}|=0.02$ Hz.

The PFR deadbands for hydropower units and thermal power units are set to be ±0.05 Hz and ±0.033 Hz, respectively. To decrease the PFR times provided by conventional SGs, the FDB of the ES inverter needs to be smaller. Therefore, once $f_{db,ES}$ is determined, the droop coefficient $k_{HD,ES}$ in

the improved triangular hysteresis area can be derived as:

$$k_{\mathrm{HD,ES}}=\frac{k_{\mathrm{D,ES}}f_{\mathrm{db,ES}}}{f_{\mathrm{db,ES}}-f_{\mathrm{hdb,ES}}} \tag{15}$$

V. Simulation

To verify the effectiveness of the FDB control methods for the GFM-ES inverter, the system depicted in Fig. 6, which includes a two-stage DC/AC converter and an SG, is simulated. The rated active power of SG $P_{\mathrm{SG,ref}}$ is scaling down to 20 kW to align with the power level of ES inverter. To enhance the PFR ability of ES inverter, the FDB of ES is set smaller than that of SG, and the main simulation parameters are shown in Table I. Notably, to suppress the power oscillation within FDB, the damping is still required within FDB, including the damping from the dual-loop control and damping control of the power loop.

TABLE I
Main Simulation Parameters

Parameter	Value
$k_{\mathrm{D,SG}}$	20 kW/Hz
Damping factor of SG D_{SG}	0.12 kW/Hz^2
J_{SG}	3 kg·m^2
FDB of SG $f_{\mathrm{db,SG}}$	±0.05 Hz
$k_{\mathrm{D,ES}}$	20 kW/Hz
C_{dc}	8×10^{-4} F
U_{dc}	750 V
$f_{\mathrm{db,ES}}$	±0.03 Hz
$f_{\mathrm{hdb,ES}}$	±0.02 Hz

A. DVSC Method

Figure 14 shows the simulation results of the DVSC method with a load disturbance of 0.2 kW at 10 s, where WDB is referred to without FDB.

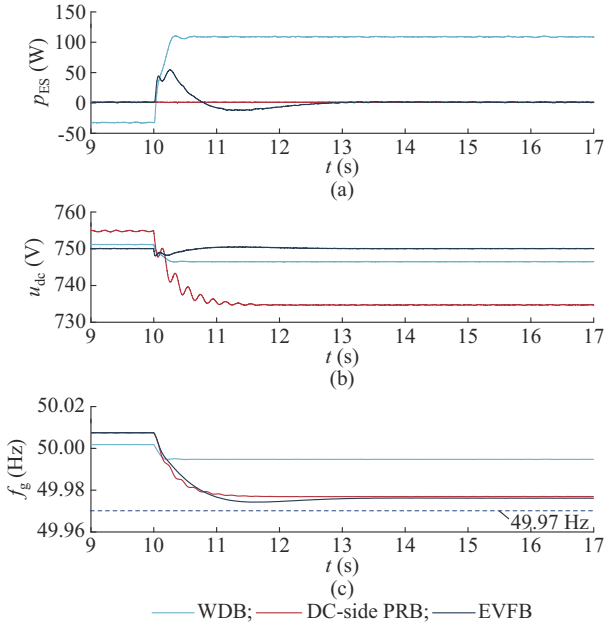

Fig. 14. Simulation results of DVSC method. (a) Active power of ES inverter. (b) DC capacitor voltage. (c) Grid frequency.

As shown in Fig. 14(c), all frequency deviations remain within the FDB. With the DC-side PRB and EVFB methods, the active power response of ES inverter for the PFR is zero in steady state, as indicated in Fig. 14(a). The output power of ES inverter is zero in the transient state with the DC-side PRB method as the IR is provided by the DC capacitor. To ensure the DC voltage variation Δu_{dc} smaller than the limit, the inertia should not be too large, and the related simulation results are shown in Supplementary Material A Fig. SA1.

B. PSC Method

The simulation results for PSC method are presented as follows with a load disturbance of 0.2 kW at 10 s.

The simulation results of droop control are depicted in Fig. 15. As previously introduced, the AC-side PRB method makes $\Delta\omega_{\mathrm{ES}}$ equal to zero within the FDB, preventing the active power response from being zero. Therefore, the droop control method can only utilize the EVFB method.

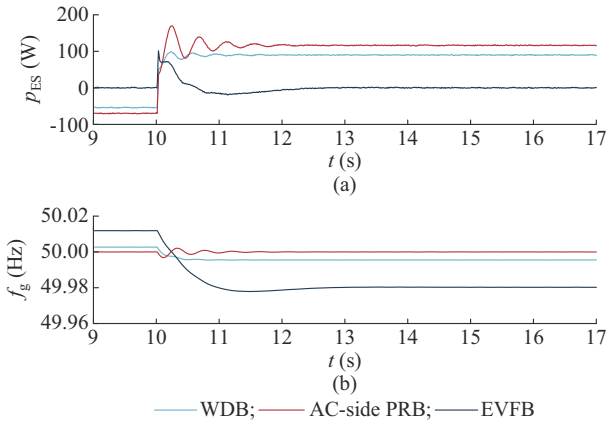

Fig. 15. Simulation results of droop control. (a) Active power of ES inverter. (b) Grid frequency.

The simulation results for VSG are shown in Fig. 16. It can be found that the power response within the FDB is zero in the steady state with the AC-side PRB and EVFB methods. A little power change is observed in the transient state due to the IR, while the AC-side PRB method has more evident IR.

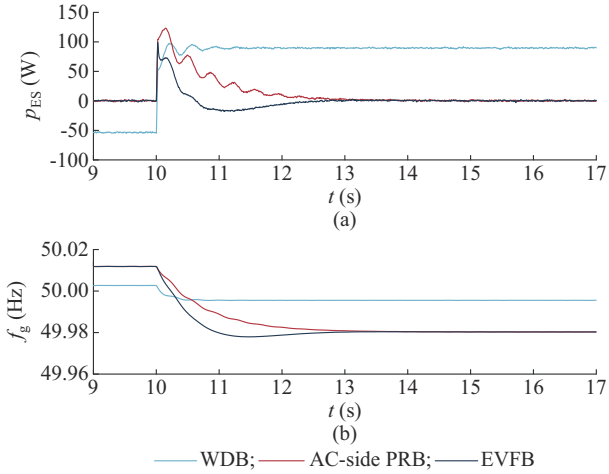

Fig. 16. Simulation results of VSG control. (a) Active power of ES inverter. (b) Grid frequency.

C. FDB Setting Methods

This subsection simulates different FDB setting methods when the ES inverter suffers a sudden load increase that causes the frequency deviation exceeding the FDB. As shown in Fig. 17, the load increases by 0.5 kW at 10 s and decreases by 0.4 kW at 14 s.

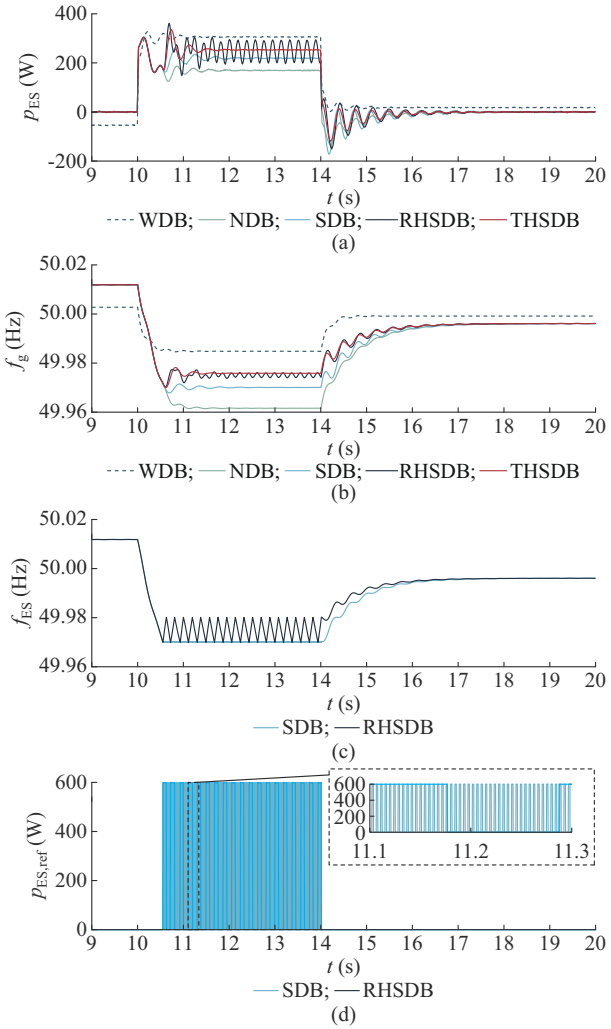

Fig. 17. Simulation results of different FDB setting methods. (a) Active power of ES inverter. (b) Grid frequency. (c) Frequency of ES inverter. (d) Power reference of ES inverter.

From Fig. 17(a) and (b), it can be observed that the NDB method weakens the PFR ability of the ES inverter, leading to a larger frequency deviation. The SDB and RHSDB methods can enhance the PFR performance; however, the SDB method converges f_{ES} to 49.97 Hz, resulting in power reference oscillations between 0 and 0.6 kW. In addition, the RHSDB method will make f_{ES} between 49.97 Hz and 49.98 Hz, contributing to power reference oscillation as shown in Fig. 17(c) and (d). This indicates that both the SDB and RHSDB methods may cause oscillations after disturbance.

The THSDB method shown in Fig. 13(d) effectively addresses the oscillation problem by preventing sudden changes in the power reference from 0 to 0.6 kW. As shown in Fig. 17(b), all of the FDB setting methods can smoothly return to the FDB area when the load decreases at 14 s.

In summary, ① the EVFB method for zero active power response within the FDB is universally applicable for the GFM-ES inverter and operates with a smaller IR; ② the PRB methods with a larger IR are beneficial for the two-stage ES inverter with the DVSC and VSG methods, but the DC-side PRB method needs to consider the deviation of DC voltage; and ③ the THSDB method for FDB setting can enhance the PFR performance of ES inverter and prevent oscillation in more situations.

VI. Experiment

To further verify the effectiveness of the FDB control methods for the GFM-ES inverter, an islanded microgrid comprised of two single-stage GFM-ES inverters is built as shown in Fig. 18. In this setup, VSG1 is used to emulate the SG, while VSG2 is utilized to validate the FDB control methods. The FDB of VSG1 is set to be zero with PFR capability, which can provide extra power demand when VSG2 is within the FDB. The main experiment parameters are shown in Table II.

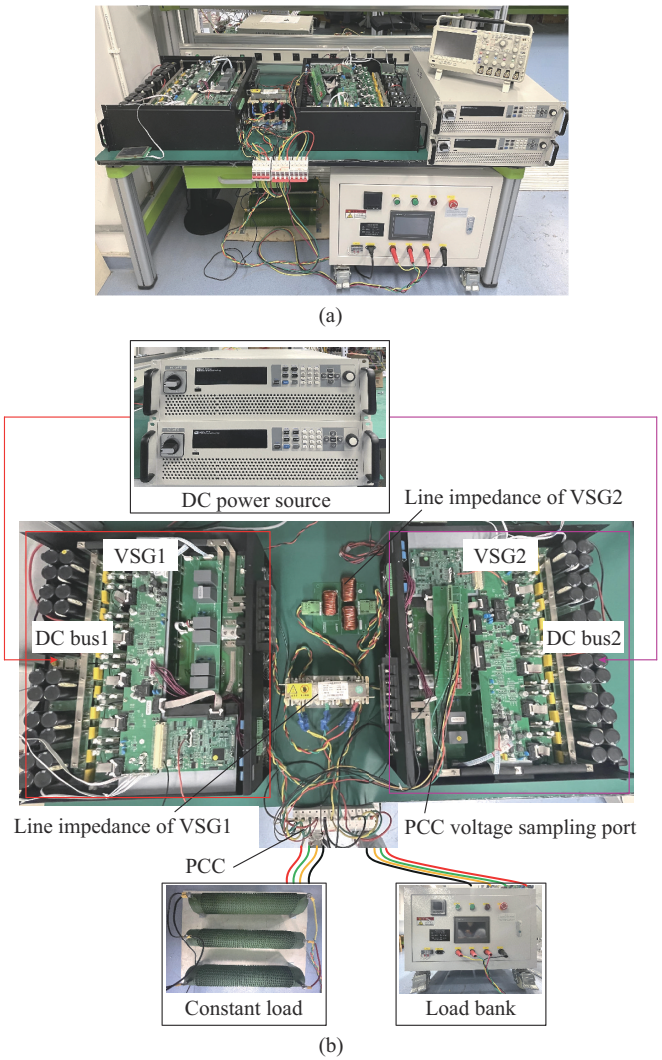

Fig. 18. Experiment platform. (a) Overview of entire platform. (b) Detailed platform structure.

TABLE II
MAIN EXPERIMENT PARAMETERS

Symbol	Definition	Value
U_g	Rated grid voltage	50 V
U_{dc}	Rated DC voltage	150 V
$P_{VSG1,ref}$	Power reference of VSG1	750 W
$P_{VSG2,ref}$	Power reference of VSG2	0 W
$k_{D,VSG1}$	Droop coefficient of VSG1	25 kW/Hz
$k_{D,VSG2}$	Droop coefficient of VSG2	25 kW/Hz
J_{VSG1}	Inertia of VSG1	1 kg·m^2
L_{VSG1}	Line impedance of VSG1	1.15 mH
L_{VSG2}	Line impedance of VSG2	0.45 mH
$f_{db,VSG2}$	FDB of VSG2	±0.03 Hz
$f_{hdb,VSG2}$	Boundary of hysteresis for VSG2	±0.02 Hz
R_c	Constant load	5 Ω

A. FDB Control Loop

Figure 19 presents the experiment results of different implementation methods for FDB with a load increasement of 0.56 kW. The active power of VSG1 and VSG2, and the grid frequency values are output via the DAC ports of digital signal processor (DSP). The active power range is set from –0.5 to 2.5 kW, and the frequency range is set from 49.9 to 50.05 Hz.

From Fig. 19, it can be observed that the grid frequency remains within the FDB. The output active power of VSG1 and VSG2 is evenly distributed for WDB, as shown in Fig. 19(a). After increasing the load, the output active power of VSG2 remains zero in the steady state with the PRB and EVFB methods, while VSG1 provides all the power, as shown in Fig. 19(b) and (c). In addition, to further verify the reliability of different implementation methods for FDB and imitate the real-world power grid, the experiment results for the voltage and current of VSG2, and a continuous load disturbance are shown in the Supplementary Material A Fig. SA2 and Fig. SA3, respectively.

From Fig. 19, it can be found that both the PRB and EVFB methods have no power response for PFR in the steady state, the PRB method provides larger IR in the transient state with a lower RoCoF as discussed in the theoretical analysis.

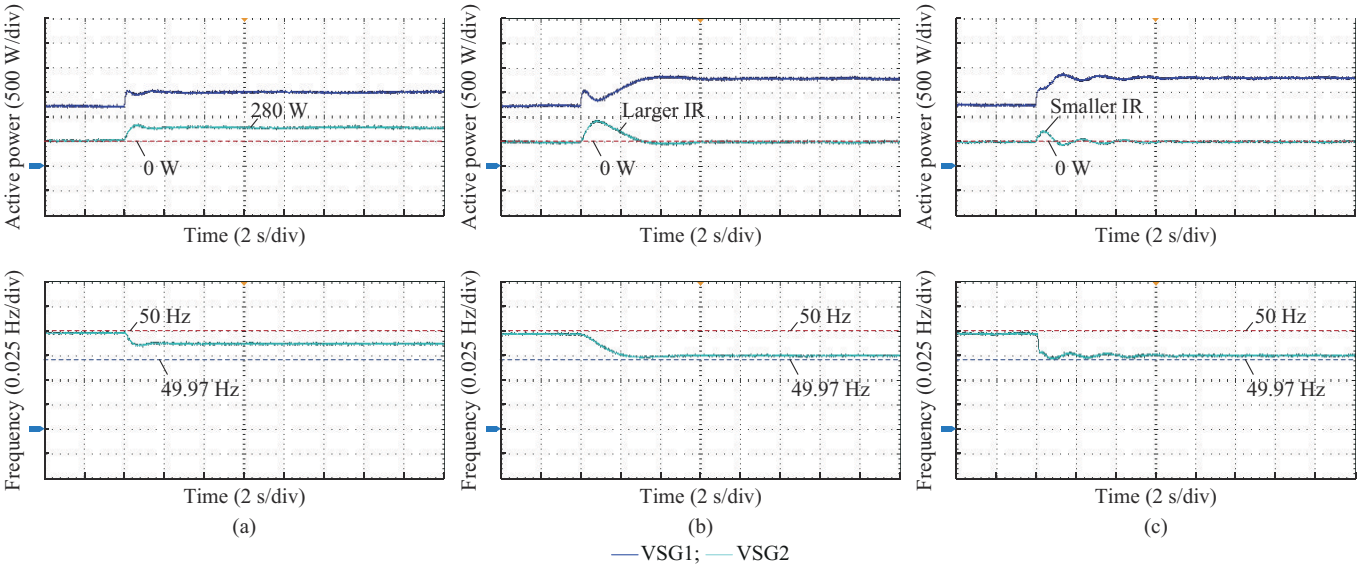

Fig. 19. Experiment results of different implementation methods for FDB. (a) WDB. (b) PRB. (c) EFVB.

B. FDB Setting Methods

This subsection conducts experiments with various FDB setting methods in response to a sudden load increase of 0.99 kW, which causes the frequency deviation to exceed the FDB. Follows this, a load decrease of 0.74 kW is set after the system reaches the new steady state to confirm that the system can return to the FDB.

From Fig. 20, it can be observed that the experimental results align closely with the simulation results. The NDB method weakens the PFR capability of VSG2, as shown in Fig. 20(b), leading to larger grid frequency deviations. Figure 20(c) demonstrates that the SDB method can enhance the PFR performance of VSG2 to a certain extent. However, this method introduces power reference oscillations as shown in Fig. 20(f), indicating oscillations in control loops. The RHSDB method can further enhance the PFR ability, as illustrated in Fig. 20(d), with a larger power response, but it still exhibits oscillations in control loops, as shown in Fig. 20(g). The experiment result in Fig. 20(e) shows the THSDB method can enhance the PFR ability of VSG2 and suppress the oscillation in control loops within the hysteresis area.

The experimental results validate the effectiveness of the PRB and EVFB methods for the implementation of FDB. Additionally, the THSDB method for enhancing the PFR capability and suppressing oscillation in control loops is also verified.

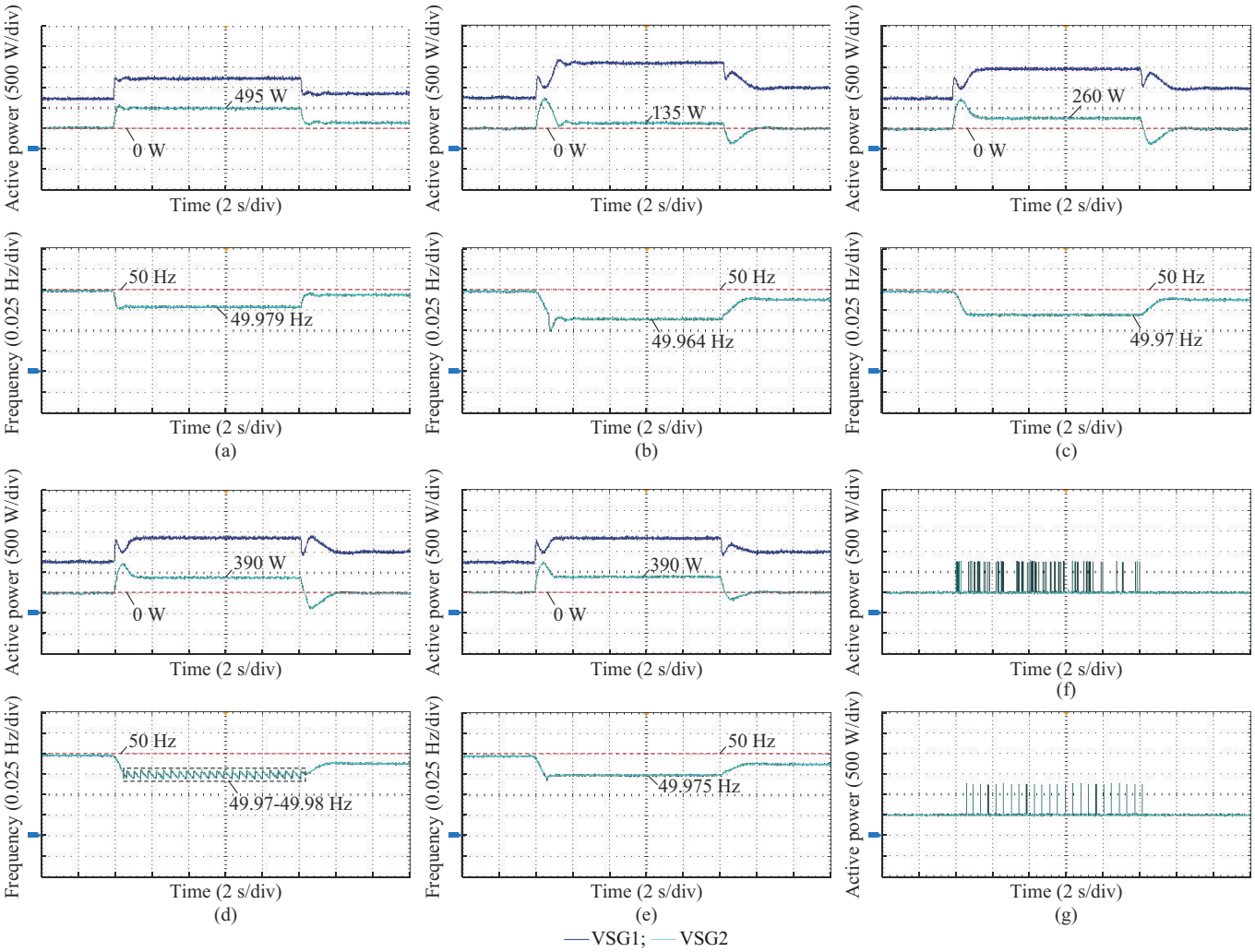

Fig. 20. Experiment results of different FDB setting methods. (a) WDB. (b) NBD. (c) SDB. (d) RHSDB. (e) THSDB. (e) Power reference of VSG2 with SDB. (f) Power reference of VSG2 with RHSDB.

VII. Conclusion

In this paper, the methods for minimizing the participation of GFM-ES inverter in PFR within the FDB are presented. In addition, the THSDB method for the FDB setting is proposed to enhance PFR capability and suppress oscillations in the FDB border. The conclusions are drawn as follows.

1) The PRB and EVFB methods are proposed for the implementation of FDB with different IR in the GFM-ES inverter. The PRB method is applicable in both DVSC and VSG methods while maintaining the IR performance. The EVFB method is universally suitable for the GFM-ES inverter with reduced IR performance. These methods can reduce ES charging cycling, thereby extending the battery's lifespan.

2) To enhance the PFR performance of ES inverter, the SDB and RHSDB methods are presented, while these methods may cause oscillations around the FDB boundary. Furthermore, the THSDB method is proposed to address oscillation, and it not only improves the PFR performance but also facilitates smoother transitions between different operating states, and reduces the risk of frequency oscillation in the FDB.

References

[1] Z. Zhang, S. Liao, Y. Sun *et al*., "A parallel-type load damping factor controller for frequency regulation in power systems with high penetration of renewable energy sources," *Journal of Modern Power Systems and Clean Energy*, vol. 12, no. 4, pp. 1019-1030, Jul. 2024.

[2] Y. Xie, H. Yi, F. Zhuo *et al*., "Analysis and stabilization for full harmonic compensation oscillation in SAPF system with source current direct control," *IET Power Electronics*, vol. 17, no. 1, pp. 107-120, Jan. 2024.

[3] Z. Wang, H. Yi, Y. Jiang *et al*., "Voltage control and power-shortage mode switch of PV inverter in the islanded microgrid without other energy sources," *IEEE Transactions on Energy Conversion*, vol. 37, no. 4, pp. 2826-2836, Dec. 2022.

[4] J. Li, Y. Qiao, Z. Lu *et al*., "Integrated frequency-constrained scheduling considering coordination of frequency regulation capabilities from multi-source converters," *Journal of Modern Power Systems and Clean Energy*, vol. 12, no. 1, pp. 261-274, Jan. 2024.

[5] O. D. Adeuyi, M. Cheah-Mane, J. Liang *et al*., "Fast frequency response from offshore multiterminal VSC-HVDC schemes," *IEEE Transactions on Power Delivery*, vol. 32, no. 6, pp. 2442-2452, Dec. 2017.

[6] D. Sun, H. Liu, F. Zhao *et al*., "Comparison of inverter generators with different support control methods," *Power System Technology*, vol. 44, no. 11, pp. 4359-4369, Aug. 2020.

[7] X. Fu, J. Sun, M. Huang *et al*., "Large-signal stability of grid-forming and grid-following controls in voltage source converter: a comparative study," *IEEE Transactions on Power Electronics*, vol. 36, no. 7, pp. 7832-7840, Jul. 2021.

[8] I. Batarseh, K. Siri, and H. Lee, "Investigation of the output droop

characteristics of parallel-connnected DC-DC converters," in *Proceedings of 1994 Power Electronics Specialist Conference*, Taipei, China, Jun. 1994, pp. 1342-1351.
[9] J. Driesen and K. Visscher, "Virtual synchronous generators," in *Proceedings of 2008 IEEE PES General Meeting – Conversion and Delivery of Electrical Energy in the 21st Century*, Pittsburgh, USA, Jul. 2008, pp. 1-3.
[10] L. Harnefors, J. Kukkola, M. Routimo *et al*., "A universal controller for grid-connected voltage-source converters," *IEEE Journal of Emerging and Selected Topics in Power Electronics*, vol. 9, no. 5, pp. 5761-5770, Oct. 2021.
[11] C. Luo, X. Ma, T. Liu *et al*., "Adaptive-output-voltage-regulation-based solution for the DC-link undervoltage of grid-forming inverters," *IEEE Transactions on Power Electronics*, vol. 38, no. 10, pp. 12559-12569, Oct. 2023.
[12] J. Fang, H. Li, Y. Tang *et al*., "Distributed power system virtual inertia implemented by grid-connected power converters," *IEEE Transactions on Power Electronics*, vol. 33, no. 10, pp. 8488-8499, Oct. 2018.
[13] W. Zhang, Z. Wang, H. Yi *et al*., "Primary frequency regulation with improved frequency deadband control of grid-forming storage inverter for longer lifespan," in *Proceedings of 2023 IEEE 2nd International Power Electronics and Application Symposium*, Guangzhou, China, Nov. 2023, pp. 1021-1026.
[14] N. Lu, J. Fang, Y. Tang *et al*., "A frequency deadband-based virtual inertia control for grid-connected power converters," in *Proceedings of 2019 10th International Conference on Power Electronics and ECCE Asia*, Busan, Korea (South), May 2019, pp. 1-6.
[15] H. Ye, W. Pei, and Z. Qi, "Analytical modeling of inertial and droop responses from a wind farm for short-term frequency regulation in power systems," *IEEE Transactions on Power Systems*, vol. 31, no. 5, pp. 3414-3423, Sept. 2016.
[16] X. Liu, B. Wu, and L. Xiu, "A fast positive-sequence component extraction method with multiple disturbances in unbalanced conditions," *IEEE Transactions on Power Electronics*, vol. 37, no. 8, pp. 8820-8824, Aug. 2022.
[17] X. Liu, L. Xiong, B. Wu *et al*., "Phase locked-loop with decaying DC transient removal for three-phase grids," *International Journal of Electrical Power & Energy Systems*, vol. 143, p. 108508, Dec. 2022.
[18] Z. Ma, X. Li, Z. Tang *et al*., "Integrated control of primary frequency regulation considering dead band of energy storage," *Transactions of China Electrotechnical Society*, vol. 34, no. 10, pp. 2102-2115, May 2019.
[19] F. Zhang, H. You, and L. Ding, "Influential mechanism modelling of dead band in primary frequency regulation of renewable energy and its coefficient correction strategy," *Automation of Electric Power Systems*, vol. 47, no. 6, pp. 158-167, Mar. 2023.
[20] L. Harnefors, M. Schweizer, J. Kukkola *et al*., "Generic PLL-based grid-forming control," *IEEE Transactions on Power Electronics*, vol. 37, no. 2, pp. 1201-1204, Feb. 2022.
[21] T. Li, Y. Li, X. Chen *et al*., "Research on AC microgrid with current-limiting ability using power-state equation and improved Lyapunov-function method," *IEEE Journal of Emerging and Selected Topics in Power Electronics*, vol. 9, no. 6, pp. 7306-7319, Dec. 2021.
[22] M. A. Zamani, A. Yazdani, and T. S. Sidhu, "A control strategy for enhanced operation of inverter-based microgrids under transient disturbances and network faults," *IEEE Transactions on Power Delivery*, vol. 27, no. 4, pp. 1737-1747, Oct. 2012.
[23] A. Pal, D. Pal, and B. K. Panigrahi, "A current saturation strategy for enhancing the low voltage ride-through capability of grid-forming inverters," *IEEE Transactions on Circuits and Systems II*: *Express Briefs*, vol. 70, no. 3, pp. 1009-1013, Mar. 2023.
[24] F. Salha, F. Colas, and X. Guillaud, "Virtual resistance principle for the overcurrent protection of PWM voltage source inverter," in *Proceedings of 2010 IEEE PES Innovative Smart Grid Technologies Conference Europe (ISGT Europe)*, Gothenburg, Sweden, Oct. 2010, pp. 1-6.
[25] Z. Wang, F. Zhuo, H. Yi *et al*., "Analysis of dynamic frequency performance among voltage-controlled inverters considering virtual inertia interaction in microgrid," *IEEE Transactions on Industry Applications*, vol. 55, no. 4, pp. 4135-4144, Jul. 2019.
[26] Z. Wang, H. Yi, F. Zhuo *et al*., "Active power control of voltage-controlled photovoltaic inverter in supporting islanded microgrid without other energy sources," *IEEE Journal of Emerging and Selected Topics in Power Electronics*, vol. 10, no. 1, pp. 424-435, Feb. 2022.

Wei Zhang received the B.S. degree from China University of Mining and Technology, Xuzhou, China, in 2022. He is currently working toward the M.S. degree in Xi'an Jiaotong University, Xi'an, China. His research interest includes control strategy of storage inverters.

Zhenxiong Wang received the B.S. and Ph.D. degrees in electrical engineering from Xi'an Jiaotong University, Xi'an, China, in 2014 and 2021, respectively. He is currently an Assistant Professor with Xi'an Jiaotong University. His research interests include inverter control in microgrid and power quality.

Yingjie Peng received the B.S. degree from Southwest Jiaotong University, Chengdu, China, in 2022. He is currently working toward the M.S. degree in Xi'an Jiaotong University, Xi'an, China. His research interests include power quality control and microgrid.

Jingting Wu received the B.S. degree from Chang'an University, Xi'an, China, in 2022. She is currently working forward the M.S degree Xi'an Jiaotong University, Xi'an, China. Her research focuses on control strategy of grid-forming inverters.

Qiru Li received the B.S. degree from Xi'an Jiaotong University, Xi'an, China, in 2022. He is currently working towards the Ph.D. degree in Xi'an Jiaotong University. His research interests include power quality control and power conversion system.

Hao Yi received the Ph.D. degree from Xi'an Jiaotong University, Xi'an, China, in 2013. He visited the Department of Energy Technology, Aalborg University, Aalborg, Denmark, from 2016 to 2017. He is currently an Associate Professor with Xi'an Jiaotong University. His research interests include power electronics technology used in power quality control, distributed power control, and grid-connected converter modeling/control.

Zebin Yang received the B.S. and Ph.D degrees from Xi'an Jiaotong University, Xi'an, China, in 2017 and 2023, respectively. Currently, he serves as an Assistant Professor at Xi'an Jiaotong University. His research interests include power quality control and distributed power control.

Li Li received the Ph.D degree in electrical engineering from Tsinghua University, Beijing, China. Currently, he serves as a Senior Engineer at State Grid Shaanxi Electric Power Company, Xi'an, China. His research interest includes power system reliability.

Fang Zhuo received the B.S., M.S., and Ph.D. degrees from Xi'an Jiaotong University, Xi'an, China, in 1984, 1989, and 2001, respectively. He received four provincial- and ministerial-level science and technology advancement awards. He is the Power Quality Professional Chairman of the Power Supply Society in China. His research interests include power electronics, power quality, and inverters for distributed power generation.